Continental J. Information Technology 4: 57 - 64, 2010 ISSN: 2141 - 4033
 http://www.wiloludjournal.com

MILLIMETER WAVE PROPAGATION FOR IMPROVED DISTRIBUTED WIRELESS COMMUNICATION SYSTEM

Biebuma J.J., Eteng A. and Elechi P.
Department of Electrical/Electronic Engineering, University of Portharcourt.

ABSTRACT
In this paper, extensive measurements are conducted in a room environment at 60GHz to analyze channel characteristics for various channel configurations. The channel parameters obtained from measurements are analyzed based on generic channel models. A single-cluster model is applied for various parameter retrieval and performance evaluations. On the basis of this model, the power delay profiles are described by a root-mean-square delay spread, K-factor and power delay profile. The channel is configured with various combinations of omnidirectional, fan-beam and pencil-beam antennas at the receiver and transmitter sides, at both line-of-sight and non line-of-sight conditions. Results show that an increase in the signal coverage and performance can be achieved by proper alignment of transmit and receive antenna beams within sight of one another. Furthermore, performance under non line-of-sight conditions can be improved by the use of directive antennas.

KEYWORDS: Fan-beam, Propagation, Channel, multigigabit, millimeter.

INTRODUCTION

With the rapid progress in telecommunications, more and more services are provided on the basis of broadband communications, such as video services and high speed internet. With the universal adoption of optical fibre-based backbone networks providing almost an unlimited communications capability, the limited throughput of the subscribers loop becomes one of the most stringent bottlenecks. Compared to the capacity of the backbone network, which is measured by tens of gigabit per second, the throughput of the subscriber loop is much lower, only up to hundreds of megabits per second for wired systems (including fixed wireless access) (Shidong *et al*, 2003). The basic problem of distributed wireless communication systems, therefore, is that the available channel bandwidth is too limited compared to the almost unlimited services requirement, just like cars jammed in a crowded narrow paths (Shidong *et al*, 2003).

Chong and Yong (2007), however, suggest that millimeter wave technology can be used to improve this low throughput of the subscribers loop. Millimeter waves generally correspond to the electromagnetic spectrum between 30GHz to 300GHz, with wavelength between one and ten millimeters. In the context of wireless communication, the term generally corresponds to a few bands of spectrum near 30GHz, 60GHz and 94GHz (Muquaibel, 2003).

This paper focuses on the 60GHz band. The characteristics for various channel configurations at 60GHz are analyzed to determine the power delay profile and the most suitable antenna configuration.

MATERIALS AND METHODS

CHANNEL THEORY

For the 60GHz radio applications in indoor environments, it is highly likely that the receiver can only be used within a single room, for example, an open office where the transmitter is located. This is occassioned by the high penetration loss caused by construction materials (Yang *et al*, 2007).

One of the biggest challenges for designing a high data rate 60GHz system is the limited link budget due to high path loss during radio propagation (Lim et al, 2007). For most 60GHz applications, the transmitter and the receiver will keep stationary, and the time variation of the channel will be introduced by moving objects due to the Doppler effect (Kvicera and Grabner, 2007). The movements of human bodies within the channel will cause significant temporal fading and shadowing effect, whose level depends on the moving speed, the number of persons, and the propagation environment. The remaining significant impact on the system caused by the radio channel is the frequency selectivity due to multipath effect, which induces intersymbol interference (ISI) in communication systems (Chong and Yong, 2007).

Multipath propagation in indoor environments is strongly affected by the dimensions of the environment and the density of furnishings. The influence of the environment on the channel can be noticed in the power delay profile (PDP), which describes the span of the received signal over time delay (Yang *et al*, 2007). For a wideband transmission system, the complex lowpass impulse response of a Rician channel is modeled as a direct or strong specular path plus *N* independent Rayleigh fading paths, which is expressed as:

$$h(t,\tau)=\alpha_0 e^{j}\phi_0(t)\delta(\tau-\tau_0)+\sum_{n-1}^{N}\alpha_n e^{j}\phi_n(t)\,\delta(\tau-\tau_n), \quad \ldots\ldots\ldots\ldots\ldots\ldots\ldots\ldots(1)$$

where $\alpha_0 e^{j}\phi_0(t)$ is the response of the direct or strong specular path which stays stationary in a local area, $\{N,\alpha_{n,}\phi_{n,}\tau_n\}$ are randomly time-varying variables: the number of multiple paths, the amplitude, phase, and arrival-time of the nth path, respectively (Yang *et al*, 2007). The time dependency of the channel is introduced by arbitrary movements of the transmitter, the receiver or other objects. Since the path number, the amplitude and the arrival-time are relatively static in a local area, the time dependency is omitted here. A Rician *K*-factor is used to characterize the Rician fading channel and defined as the ratio between the powers contributed by the steady path and the scattered paths, that is

$$K=\frac{E\left\{\left|\alpha_0\right|^2\right\}}{2\sigma^2} \quad \ldots\ldots\ldots\ldots\ldots\ldots\ldots\ldots\ldots\ldots\ldots\ldots\ldots\ldots(2)$$

where $2\sigma^2$ is the mean power of the scattered paths (Nan *et al*, 2007).

MEASUREMENTS

A vector network analyzer (HP 8510C) was employed to measure complex channel frequency responses. During measurement, the step sweep mode was used with a sweep time of 20 seconds for each measurement. Channel impulse responses were obtained by inverse Fourier transforming the frequency responses generated by the continuous wave frequency generator into time domain after a Kaiser window was applied with a sidelobe level of −44dB. Three types of vertical polarized antennas with different radiative patterns, namely: omnidirectional, fan-beam and pencil-beam antennas; were applied in the measurements. Parameters of these antennas are listed in Table 1.

Table 1: Antenna parameters

Types of Antennas	Half Power Beamwidth (^{o})		Gain (dBi)
	E-plane	H-plane	
Fan beam	12.0	70.0	16.5
Pencil beam	8.3	8.3	24.4
Omnidirectional	9.0	omnidirectional	6.5

Two groups of measurements were conducted in rooms A and B separately. Both rooms have a similar structure. The windows side consists of window glasses with a metallic frame one meter above the floor and a metallic heating radiator below the window. The concrete walls are smoothly plastered and the concrete floor is covered with linoleum. The ceiling consists of aluminium plates and light holders. Some large metallic objects, such as cabinets, were standing on the ground. In room A, three aligned metallic cabinets are standing in the middle of the room and two metallic cable boxes with a height of 3.2m are attached to the brick wall side 2. The space between cabinets and ceiling was blocked using aluminium foil for the ease of the measurement analysis. Figure 1 is a plan view of the measurement rooms. Table 2 lists the measurement system configurations. In room A, at both the transmitter and the receiver side, we used the same type of omnidirectional antennas.

Three height differences of TX-RX were considered, namely, 0.0, 0.5 and 1.0m (denoted by $OO_{0.0}$, $OO_{0.5}$, and $OO_{1.0}$ for three cases, respectively.). Both line-of-sight (LOS) and non-LOS (NLOS) channels were measured in room A. In room B, a sectoral horn antenna with fan-beam pattern was applied at the TX side and located in a corner of the room at the height of 2.5m. At the RX side, three types of antennas with omnidirectional, fan-beam, and pencil-beam patterns at the height of 1.4m. The three TX/RX combinations are denoted by FO, FF, and FP, respectively, in which of the latter two cases the TX/RX beams are directed towards each other. In

addition, we measured the channels for the cases of FF and FP with TX/RX beams misaligned by ±35° (denoted by $FF_{\pm 35^\circ}$ and $FP_{\pm 35^\circ}$). In room B, only LOS channels were measured.

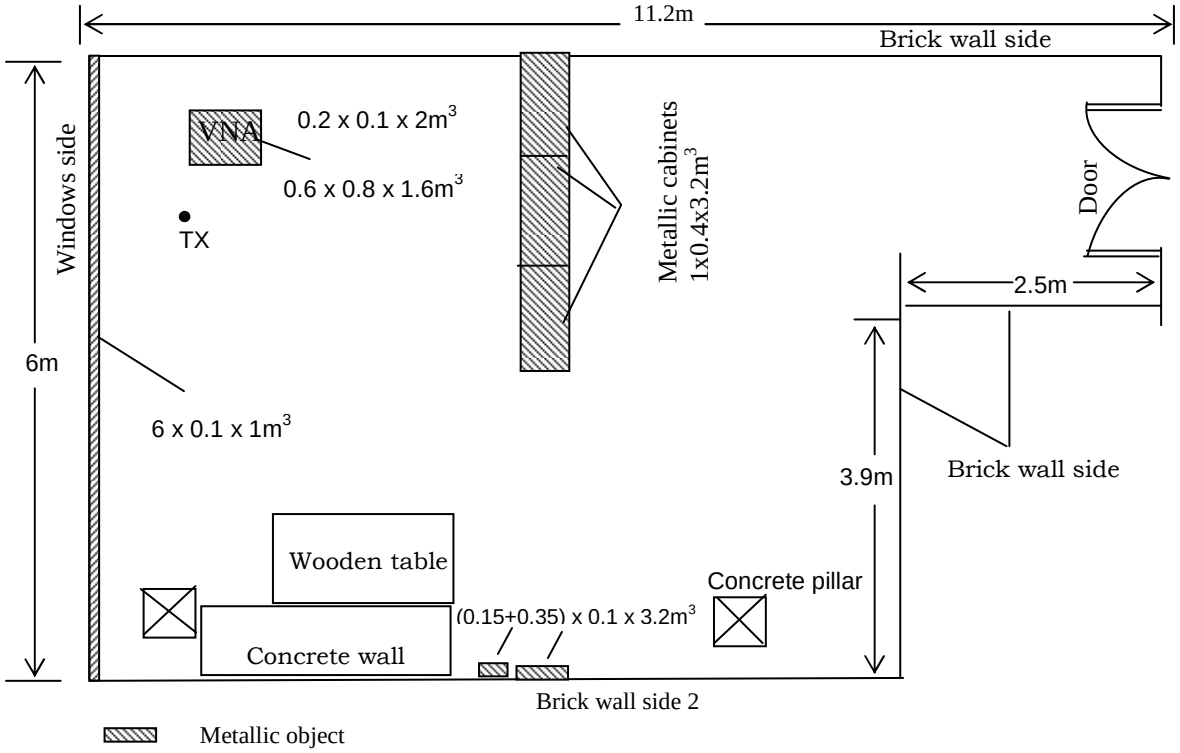

(a) Room A

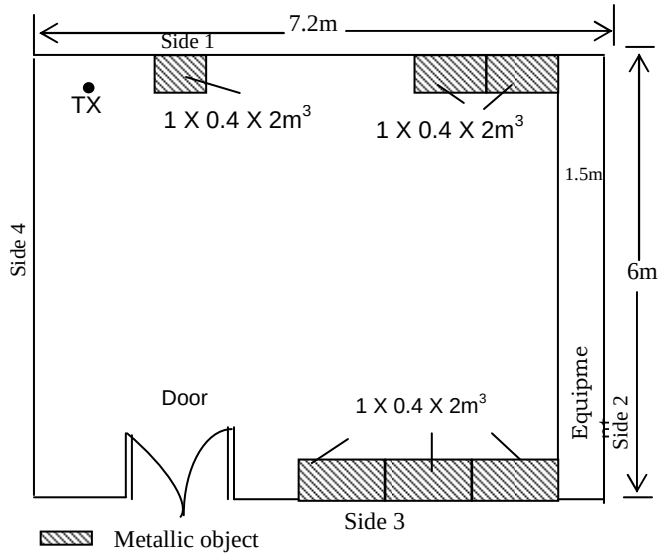

(b) Room B

Figure 1: Plan View of the rooms.

Table 2: Measurement configurations.

Rooms	Frequency Range (GHz)	Antenna (TX/RX)			
		TX	RX	Height (m)	
A	57-63	Omn	Omn	1.4/1.4	$OO_{0.0}$
				1.9/1.4	$OO_{0.5}$
				2.4/1.4	$OO_{1.0}$
B	58-62	Fan	Omn	2.5/1.4	FO
			Fan	2.5/1.4	$FF,FF_{\pm 35}$
			Pen	2.5/1.4	$FP,FP_{\pm 35}$

The results obtained are plotted in scatter diagrams which reveal the behaviour of the various parameters under different configurations. During measurement, the transmitter and receiver were kept stationary and there were no movement of persons in the rooms.

RESULTS

Using the Friis propagation rule, the received power from the transmitter is related to the path loss as:

$$P_r=P_t+G_t+G_r-PL_{(d)}\ldots\ldots\ldots\ldots\ldots\ldots\ldots\ldots\ldots 3$$

Where P_t is the transmitter power, G_t and G_r are the antenna gains at the transmitter and receiver side respectively and $PL_{(d)}$ is the free space path loss. Expressing the path loss over the log-distance:

$$PL_{(d)}= 20\log\left(\frac{4\pi r^n}{\lambda}\right) + X_\Omega\,(dB)\ldots\ldots\ldots\ldots\ldots 4$$

Where λ is the wavelength, r is the distance between the transmitter and the receiver and X_Ω denotes a zero mean Gaussian distributed random variable with a standard deviation Ω.

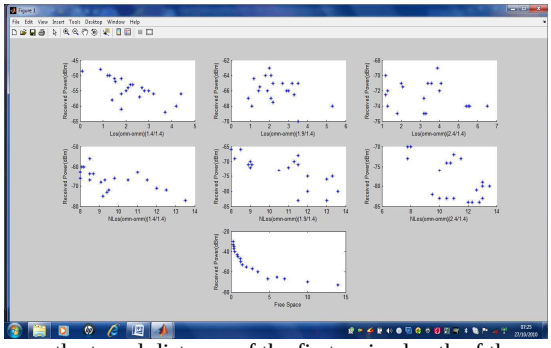

Figure 2: The received power over the travel distance of the first arrived path of the omnidirectional antenna, when the transmit power is 0 dBm

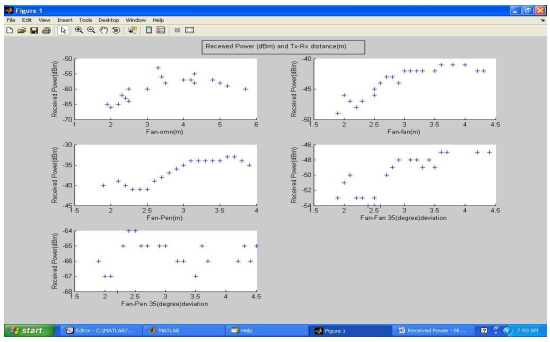

Figure 3: The received power over the travel distance of the first arrived path for the directive antenna, when the transmit power is 0dBm

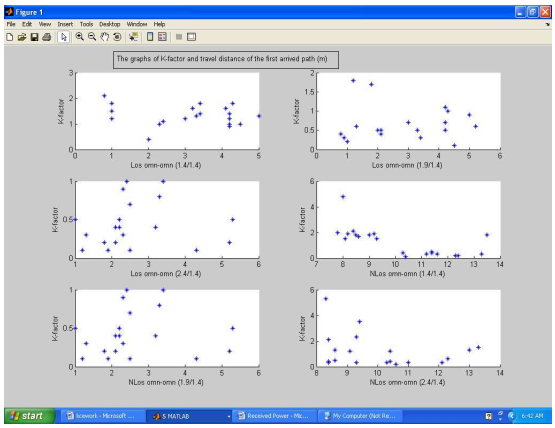

Figure 4: The measured instantaneous K-factor over the travel distance of the first arrived path of the omnidirectional antenna.

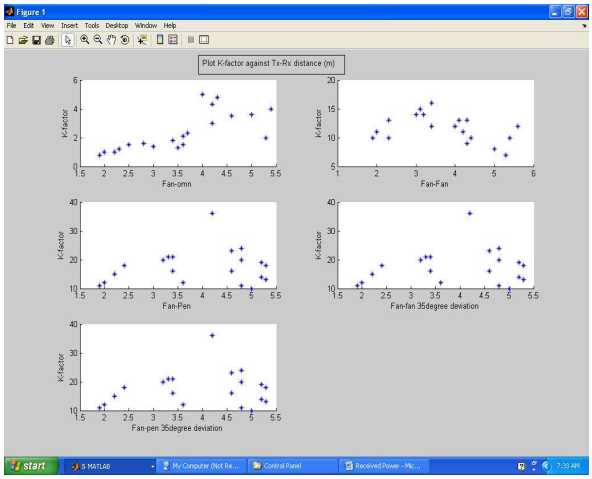

Figure 5: The measured instantaneous K-factor over the travel distance of the first arrived path of the directive antenna.

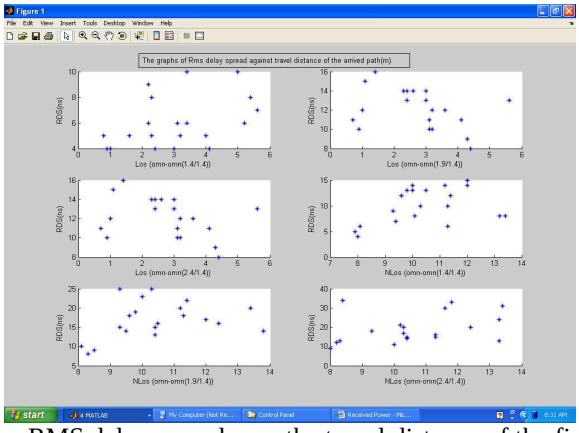

Figure 6: The instantaneous RMS delay spread over the travel distance of the first arrived path.

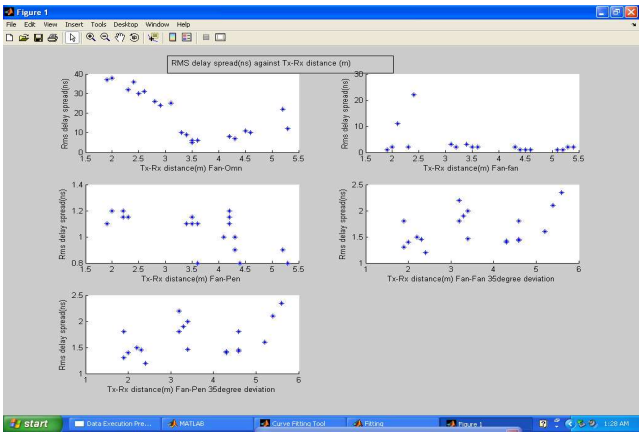

Figure 7: The instantaneous RMS delay spread over the travel distance of the first arrived path of the directive antennas.

DISCUSSION

RECEIVED POWER

Figure 2 shows the measured power level at the receiver for various antenna configurations when a unit power (0 dBm) is transmitted. Note that the x-axis of each subplot is the travel distance of the first arrived wave, that is, the direct wave for the LOS case and the first reflected wave for the NLOS case. The scattered data can be better fitted by the log-distance model since the first arrived wave will have the most significant contribution to the arrived power. Due to the highly reflective environment, the free space curve gives the accurate data for the omnidirectional configuration.

For the directive antenna configuration in figure 3, the power level is much higher and the scattered points strongly assumes a definite path except those close to the transmitter that are very sensitive to the unintentional beam pointing errors. When the receiver beams are misaligned intentionally by ±35˚ over the boresight, the received power by the fan-pen configuration will drop about 27dB due to narrower antenna beam, compared to the 5dB drop by the fan-fan one as shown in figure 3. From our observation, the 35˚ misalignment is about half the beamwidth of the fan-beam antenna and thus the direct path is still within the sight. It appears that the loss exponents are much smaller than the free-space exponent for the omn-omn configurations but approximately equal to 2 for the directive ones.

K-FACTOR AND ROOT MEAN SQUARE DELAY SPREAD

The root mean square delay spread is calculated from the delay profile with a dynamic range fixed at 30dB. For the directive configurations of fan-fan and fan-pen, as the result of the significant suppression of multipath waves, it is observed in figures 5 and 7 that most of the channel parameters are in the region of $K > 10$, $\sigma_{\tau} < 1.5$ns, $B_{c0.5} > 400$MHz, and $B_{c0.9} > 40$MHz. where $B_{c0.5}$ and $B_{c0.9}$ are the coherence bandwidth at the correlation levels 0.5 and 0.9 respectively. When the TX/RX beams are not pointing to each other, the beam-pointing errors, for instance the 35˚ -misalignment for the Fan-Pen configuration, can seriously worsen the channel condition in terms of large root mean square delay spreads and the enormous drop of received powers, K-factors and coherence bandwidth. This implies that channel configurations with wider beams are less sensitive for beam-pointing errors. That means, the width of the beam has to be properly designed to prevent an enormous drop of channel quality caused by beam-pointing errors. In practice, multiple antennas can be deployed and beamforming algorithms will be used to achieve higher gain and suppress multipath effect by steering the main beam to the direction of the strongest path.

When an omnidirectional antenna is used at transmitter or receiver side, most of the channel parameters are in the region of $K < 3$, $\sigma_{\tau} > 5$ns, $B_{c0.5} < 200$MHz and $B_{c0.9} < 20$MHz (figures 4 and 6). The K-factors in the LOS case are generally small because of the highly reflective environment, which is to say that it low fading. Under the NLOS condition, channel parameters are strongly variant depending on the position of the receiver, due to the absence of the direct path. The coherence bandwidths at level 0.9 can be related to the root-mean-square delay spreads by $\sigma_{\tau} \times B_{c0.9} = 0.063$, while the mean values of $\sigma_{\tau} \times B_{c0.5}$ are highly variant for different configurations.

POWER DELAY PROFILE SHAPE

Taking the average over all the measured profiles for each configuration, each individual profile is normalized by its total received power. From these averages:

(1) When the TX/RX beams are aligned to each other under the LOS condition, the average delay profile consists of a direct ray and an exponentially decaying part.

(2) Under the NLOS condition, the average delay profile will be exponentially decaying without a constant part, due to the lower dependency of antenna pattern and misalignment.

(3) When the TX/RX beams are strongly misaligned and out of sight to each other, a constant level part will appear before an exponentially decaying part. Hence the average delay profile can be regarded as a function of excess delay that consists of a direct part, a constant part and a linear decaying part.

MAXIMUM EXCESS DELAYS AND NUMBER OF MULTIPATH COMPONENT

Within the dynamic range of 30dB of power delay profile, the maximum excess delay τ_{max} and the number of multipath components N are determined. The values of τ_{max} are distributed within 10 to 170ns and so is the values of N within 3 to 100, depending on the channel configurations. For all the measured profiles, the number of paths per nanosecond, N/τ_{max}, has a mean value of 0.3 with a standard deviation of 0.06 showing that there is minimum delay using the 60GHz band.

CONCLUSION

Based on the analysis conducted, the following conclusions can be drawn.

(1) The TX/RX antenna beams have to be properly aligned within the sight of each other, else the beam-pointing errors will cause an enormous drop in the channel quality. The wider beam antennas are less sensitive for beam-pointing errors, which indicates that a proper beamwidth has to be designed in practice.

(2) To increase the signal coverage and performance in the NLOS area, it is preferable to apply directive antennas.

(3) When an omnidirectional antenna is used at TX or RX side in a LOS case, the channel parameters are generally small because of the reflective environment.

(4) The measurement results have shown that the use of high gain antenna can significantly reduce the delay spread of the distributed wireless communication system channel when the transmitter and receiver antennas are aligned.

RECOMMENDATION

Based on the above analysis and results obtained, it can be observed that millimeter wave propagation has the potentials to provide the next generation multigigabit wireless communication system.

Further research work could be aimed at understanding the link budget, the effects of rain-induced bistatic scattering, and the effects of atmospheric oxygen, humidity and fog in millimeter wave propagation.

REFERENCES

Chong C. C. and Yong S. K. (2007): An overview of multigigabit wireless through millimeter wave technology: potentials and technical challenges. EURASIP Journal, 2007 (1): 3 – 6.

Kvicera V. and Grabner M. (2007): Rain Attenuation at 58 GHz: Prediction versus Long-Term Trial Results, EURASIP Journal, 2007 (5): 3-6.

Lim C.P, Lee, M., Burkholder R.J., Volakis J.L., Marhefka, R.J. (2007): 60 GHz indoor propagation studies for wireless communication based on Ray-tracing method, EURASIP Journal, 2007 (3): 2 – 3.

Muqaibel A.H. (2003): Characterization of ultra widespread communication channels, Ph.D dissertation, Virginia polytechnic Institute and state University, Blacksburg, Va, USA.

Nan G., Qui, R.C., Mo S.S. and Yakahashi K;, (2007): 60 GHz Milliimeter-wave Radio: Principle, Technology, and new Results, EURASIP Journal, 2007 (2): 3-5.

Shidong Zhou, Ming Zhao, Xibin Xu, Jing Wang and Yan Yao (2003): Distributed wireless communication system: A new Architecture for future public wireless access, IEEE Communications magazine, E03-R: 108 – 113.

Yang H, Smulders P.F.M. and Herben M.H.A.J. (2007): Channel characteristics and Transmission performance for various channel configurations at 60GHz, EURASIP Journal, 2007 (4): 3-5.

Received for Publication: 01/11 /2010
Accepted for Publication: 02/12 /2010

Corresponding Author
Elechi P
Department of Electrical/Electronic Engineering, University of Port Harcourt.
E-mail: elechipromise@yahoo.com